
InnerQ: Hardware-Aware Tuning-Free Quantization of KV Cache for Large Language Models

Mohammadreza Tayaranian* Amir Ardakani Warren J. Gross
Department of Electrical and Computer Engineering
McGill University
Montreal, QC, Canada

Abstract

When transformer-based language models are deployed for text generation, most of the inference time is spent in the decoding stage, where output tokens are generated sequentially. Reducing the hardware cost of each decoding step is therefore critical for efficient long-context generation. A major bottleneck is the key-value (KV) cache, whose size grows with sequence length and often dominates the model’s memory footprint. Prior work has proposed quantization methods to compress the KV cache while minimizing its loss of precision. We present InnerQ, a hardware-aware KV cache quantization scheme that reduces decode latency without compromising evaluation performance. InnerQ performs group-wise quantization by grouping cache matrices along their inner dimension. This grouping strategy aligns dequantization with vector-matrix multiplication and increases data reuse across GPU compute units. As a result, InnerQ reduces memory access and accelerates dequantization, achieving an average $1.3\times$ speedup over prior KV cache quantization methods and $2.7\times$ over the non-quantized baseline. To maintain fidelity under aggressive compression, InnerQ incorporates three techniques: (i) hybrid quantization, which chooses symmetric or asymmetric quantization for each group based on local statistics; (ii) high-precision windows for both recent tokens and attention sink tokens to mitigate outlier leakage; and (iii) per-channel normalization of the key cache, computed once during prefill and folded into the model parameters to eliminate runtime overhead. Beyond reducing latency, experiments on Llama and Mistral models show that InnerQ also improves few-shot evaluation scores relative to prior KV cache quantization methods.

1 Introduction

Large language models (LLMs) are increasingly deployed in text generation applications, including chatbots, many of which require processing long token sequences and therefore impose a growing demand on inference-time compute and memory resources. Improving the efficiency of text generation is therefore essential for reducing power consumption and enabling deployment on resource-constrained edge devices. A key contributor to generation cost is the decode phase, in which output tokens are produced autoregressively, one token at a time [16].

To improve decoding efficiency, modern LLMs commonly use KV caching [15], which stores the key and value matrices of previous tokens and restricts computation at each step to the newest token. This mechanism reduces redundant computation and improves throughput. However, because the cache grows linearly with the number of processed tokens, its memory footprint increases to the point where KV cache dominates the memory footprint of the model [13]. The growing size and hardware

*Correspondence to mohammadreza.tayaranian@mail.mcgill.ca

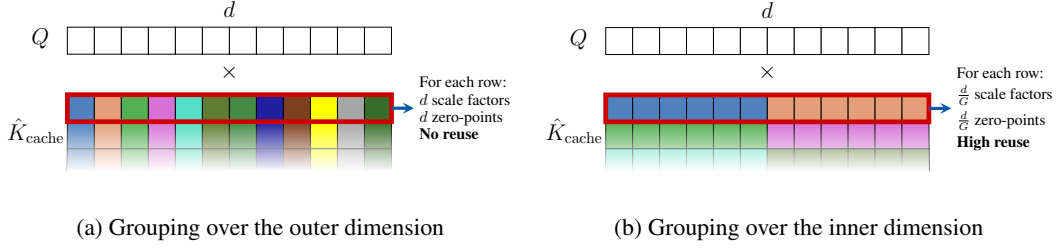


Figure 1: Visualization of the vector-matrix multiplication between the floating-point vector Q and the quantized matrix \hat{K}_{cache} in an illustrative example. Cells with the same color are in the same quantization group and share a scale factor and zero point. A similar visualization is true for the vector P and the quantized matrix \hat{V}_{cache} .

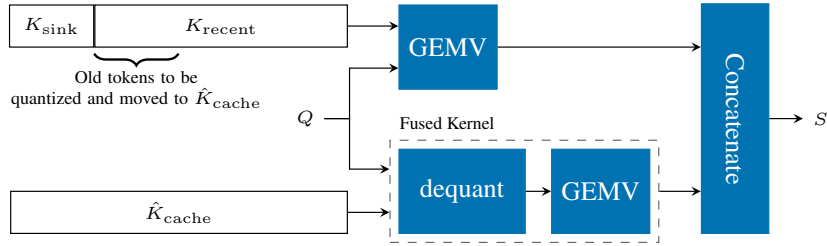


Figure 2: Overall schematics of using our proposed KV cache quantization method in the attention computation process (Equation 3). The value cache has a similar behavior. A small high-precision window consisting of sink tokens (K_{sink}) and recent tokens (K_{recent}) is maintained along with the quantized kernels (\hat{K}). The portions of the output corresponding to the quantized kernel and the full-precision windows are computed separately and then merged.

footprint of the KV cache makes its compression a critical requirement for efficient long-sequence generation.

Previous work has proposed KV cache quantization as an effective compression strategy for reducing memory usage during decoding [14, 11, 9, 20]. To better understand existing designs, consider the vector-matrix multiplication $C = AB$, where $A \in \mathbb{R}^{1 \times K}$ is a floating-point vector and $B \in \mathbb{R}^{K \times N}$ is a quantized matrix. Depending on the operation, A represents either the query or the attention weights, while B represents either the key or the value matrix. Existing methods apply group-wise quantization to B by partitioning it into small groups, each with its own scale factor [14, 20]. To preserve quantization accuracy, these groups are typically formed along the outer dimension, i.e., N , which helps isolate large outliers and reduce their effect on precision [14, 20].

However, outer-dimension grouping is not well matched to the execution pattern of quantized vector-matrix multiplication on GPUs. In this operation, each row of the cache matrix is first dequantized and then multiplied by the floating-point vector. When groups are formed along the outer dimension, the entries within a row belong to different quantization groups and must be dequantized separately (Figure 1a). In contrast, inner-dimension grouping allows compute units to reuse scale factors across multiple compute units, reducing memory access, improving data reuse, and ultimately lowering the latency of the quantized vector-matrix multiplication (Figure 1b).

Building on this intuition, we propose InnerQ, a tuning-free, hardware-aware KV cache quantization method for efficient LLM decoding. InnerQ is designed to reduce inference latency in text generation with quantized KV cache while preserving evaluation performance. It provides three quantization variants, InnerQ_{Base}, InnerQ_{Hybrid}, and InnerQ_{Small}, which trade off evaluation performance, cache size, and speedup. To achieve this balance, we incorporate the following techniques into different InnerQ variants:

- **Inner Dimension Grouping:** We apply group-wise quantization to the KV cache by forming groups along the *inner* dimension of the cache matrices. As discussed earlier, this grouping strategy reduces memory access and speeds up dequantization. Experiments in

Section 5.3 demonstrate that inner-dimension grouping, adopted by all InnerQ variants, reduces decoding latency compared to KIVI [14], which groups KV cache matrices along the outer dimension. This highlights inner-dimension grouping as a key design choice for efficient quantized KV caching.

- **High-precision Windows:** Inspired by prior work [14, 20, 5, 22], InnerQ retains a small subset of cache tokens in half-precision. Unlike KIVI [14], which allocates the entire high-precision window to the most recent tokens, InnerQ reserves part of this budget for the first few tokens in the sequence. These initial tokens often act as *attention sinks*, receiving disproportionately high attention scores throughout generation. This design preserves the attention sink tokens and prevents their influence from leaking into the quantization groups and diminishing the precision of other tokens [17, 22].
- **Per-channel Normalization of Key Cache:** To reduce the magnitude of outliers, InnerQ applies channel-wise normalization to the key cache. The normalization factors are computed during the prefill stage and folded into the key and query weights, thereby avoiding any additional runtime overhead. Token-wise grouping of the key cache makes per-channel normalization straightforward, whereas outer-dimension grouping makes it less natural and more costly to integrate.
- **Hybrid Quantization:** Symmetric and asymmetric quantization are the most prominent quantization methods used in the KV cache. In short, symmetric quantization centers the data around zero while asymmetric quantization shifts the data to the positive range before quantization. However, as discussed in Section 6.3, we observe that, given their inherent assumptions about the underlying data distribution, these quantization modes sometimes fail to maintain KV cache precision. Notably, the value cache suffers from precision loss when quantized using asymmetric quantization in low-bit regimes. To avoid a costly hyperparameter search, we propose a hybrid quantization scheme that allows each quantization group in the value cache to dynamically select either symmetric or asymmetric quantization based on the values in that group. Our experiments show that, compared to non-adaptive quantization modes, hybrid quantization improves the evaluation score of quantization in low-bit regimes (Section 5.1) with a negligible effect on latency (Section 5.3).

We evaluate InnerQ on Llama [19, 7] and Mistral [10] models of varying sizes and measure the resulting evaluation performance under KV cache quantization. As detailed in Section 5.1, InnerQ achieves average evaluation scores comparable to those of the non-quantized KV cache and prior KV cache quantization methods. We also implement fused CUDA kernels for quantized KV cache operations and measure their latency on an NVIDIA Jetson edge platform. Our measurements, discussed in Section 5.3, show that InnerQ achieves an average speedup of $2.7\times$ relative to a non-quantized FP16 cache. We also compare the latency of InnerQ with prominent KV cache quantization methods KIVI [14] and TurboQuant [23] and observe an average speedup of $1.3\times$ and $1.2\times$, respectively.

2 Related Work

KIVI [14] is one of the earliest works that proposes a tuning-free KV cache quantization method. It cites channel outliers as the main challenge in KV cache quantization and proposes an asymmetric quantization over the *outer* dimension of the key and value matrices to address this challenge. While we also propose a tuning-free quantization method with minimal overhead, we focus on quantizing the KV cache over the *inner* dimension to achieve higher speed up.

TurboQuant is a recent tuning-free, data-oblivious vector quantization method for high-dimensional vectors, including KV cache representations [23]. It applies a random rotation to the input vectors so that the rotated coordinates follow a concentrated Beta distribution, and then quantizes these coordinates using optimal non-uniform scalar quantizers [23]. The corresponding codebooks are obtained by solving an optimization problem for each target bit-width and can be precomputed, avoiding data-dependent calibration. This design differs from InnerQ, which applies uniform group-wise quantization to the KV cache; TurboQuant instead relies on non-uniform coordinate-wise quantization after random rotation, with an effective KV cache precision of 3.5 bits, obtained by assigning different bit-widths to outlier and non-outlier channel sets. Based on our experimental

results, InnerQ achieves a comparable evaluation score to TurboQuant (Section 5.1) while having a lower latency (Section 5.3).

GEAR [11] uses low-rank decomposition alongside quantization to address the outlier challenge. Despite its low accuracy drop, its need to solve small optimization problems for the low-rank decomposition leads to runtime overhead. It proposes a CUDA implementation to further mitigate this overhead. SQuat [20] proposes to minimize the quantization error by quantizing the key matrix such that its quantization error is orthogonal to the query. Building on KIVI, SQuat requires solving an optimization problem periodically to find the orthogonal matrix. Similar to GEAR, this extra optimization leads to improved accuracy, while negatively affecting the throughput of the quantized attention. Unlike GEAR and SQuat, our proposed method does not add extra steps to the quantization and is shown to have negligible overhead compared to KIVI.

KVQuant [9] proposes a non-uniform quantization where the quantization signposts are learned for each tensor. It uses a calibration dataset to compute the fisher matrix and find the signposts before inference begins. SKVQ [5] uses per-token group-wise quantization with dynamic clipping for both key and value. In other words, while the key cache is quantized over the inner dimension, the value cache is quantized over the outer dimension. Similar to our work, they propose to keep the most recent tokens in floating-point for higher precision. To overcome outlier channels, SKVQ proposes a custom ordering of channels. The optimal ordering of channels is found by gathering features of channels on a calibration dataset and clustering similar channels together for a smoother quantization. They also propose a variable group size which enables them to group similar channels together. However, whether their variable group size efficiently uses resources on a general-purpose GPU is not demonstrated by the authors. While calibration is an important step for both SKVQ and KVQuant, it leads to extra overhead and also makes their method reliant on external data. Unlike these methods, our proposed method dynamically adapts to data with hybrid quantization (Section 4.1.2) and does not require any extra calibration.

3 Background

3.1 General Notation

Let $A \in \mathbb{R}^{M \times K}$ be a matrix. We adopt a slicing notation analogous to that used in array-based libraries like PyTorch, where the i -th row and the j -th column of A are denoted by $A_{i,:}$ and $A_{:,j}$, respectively. For indices $i_1 \leq i_2$, we denote by $A_{i_1:i_2,:}$ the submatrix consisting of rows i_1 through i_2 (inclusive). Similarly, for indices $j_1 \leq j_2$, the submatrix consisting of columns j_1 through j_2 (inclusive) is denoted by $A_{:,j_1:j_2}$. The notation $A_{i_1:,}$ refers to the submatrix formed by rows i_1 through M , while $A_{:,i_1}$ denotes the submatrix consisting of rows 1 through i_1 , both inclusive. Given matrices $A \in \mathbb{R}^{N \times K}$ and $B \in \mathbb{R}^{M \times K}$, their vertical concatenation (along the first dimension) is denoted by $[A; B] \in \mathbb{R}^{(N+M) \times K}$. This notation extends naturally to higher-dimensional arrays, where slicing along each axis follows the same convention.

3.2 KV Caching

Multi-head attention (MHA) is one of the building blocks of transformer-based large language models. It starts by transforming the hidden states h into $Q \in \mathbb{R}^{n_h \times N_Q \times d_h}$ and to K and $V \in \mathbb{R}^{n_h \times N_K \times d_h}$ as

$$Q = hW_Q \tag{1}$$

$$K = hW_K \quad V = hW_V \tag{2}$$

where n_h is the number of attention heads and d_h is the head dimension. It then computes the attention matrix, $O \in \mathbb{R}^{N_Q \times d}$, as

$$S = QK^\top \tag{3}$$

$$P = \text{softmax} \left(\frac{S}{\sqrt{d_h}} \right) \tag{4}$$

$$O = PV \tag{5}$$

where $d = n_h \times d_h$ is the hidden dimension of the model.

When a language model is used for language generation its operation, is divided into two stages of *prefill* and *decode*. During the prefill stage, the hidden states $h \in \mathbb{R}^{N_Q \times d}$ contain multiple tokens that help the model obtain the context of the current task. After prefill, the model enters the decode stage where it generates tokens one by one ($N_Q = 1$). Despite that, key and value matrices contain all the context from the prefill stage and the decode stage up to that point ($N_K > 1$).

Since these matrices grow with every new token, KV caching proposes to cache and reuse key and value matrices to avoid their recomputation for each step. KV cache matrices are initialized at the end of the prefill stage as

$$K_{\text{cache}} = K \quad V_{\text{cache}} = V \quad (6)$$

and are re-used for the subsequently generated tokens so that at each step of the decode phase the key and value are computed only for the last token. Using KV caching, Equation 2 is re-written as

$$K = [K_{\text{cache}}; hW_K] \quad V = [V_{\text{cache}}; hW_V]. \quad (7)$$

After each decode step, the cache is updated with the most recently computed key and value. This technique speeds up the generation process by avoiding the full linear transformation that creates the full K and V for each token.

3.3 KV Cache Quantization

Previous work has proposed quantizing the KV cache to reduce its memory footprint. Given that both K and V are multiplied by full-precision matrices, KV cache quantization methods store them in low-precision data types, but dequantize them before the matrix multiplications of Equations (3) and (5). Applying quantization to the KV cache, Equation (6) is reformulated as

$$\hat{K}_{\text{cache}} = \text{quant}(K) \quad \hat{V}_{\text{cache}} = \text{quant}(V) \quad (8)$$

and Equation (7) is replaced by

$$K = [\text{dequant}(\hat{K}_{\text{cache}}); hW_K] \quad V = [\text{dequant}(\hat{V}_{\text{cache}}); hW_V]. \quad (9)$$

where \hat{K}_{cache} and \hat{V}_{cache} are quantized cache matrices.

4 Methodology

4.1 Quantization Scheme

We propose to use b -bit group-wise quantization to quantize $K, V \in \mathbb{R}^{n_h \times N_K \times d_h}$ with a group size G . Each matrix is divided into smaller quantization groups where each group has a scale factor and zero-point (if applicable).

We begin by describing the symmetric and asymmetric quantization modes and then describe our proposed hybrid quantization mode. Although K and V are interchangeable in the equations and definitions, we use K throughout for ease of reading. Without loss of generality we assume that K is grouped over the inner dimension ($d_h \equiv 0 \pmod{G}$).

4.1.1 Asymmetric and Symmetric Quantization

Group-wise asymmetric quantization represents each tensor using a scale factor and a zero-point. Let $S \in \mathbb{R}^{n_h \times N_K \times \frac{d_h}{G}}$ and $Z \in \mathbb{R}^{n_h \times N_K \times \frac{d_h}{G}}$ denote the corresponding scale factor and zero-point matrices, respectively. The quantized value of the element for head i , token j , and channel k of K is then given by

$$\hat{K}_{i,j,k} = \text{quant}_{\text{asym}}(K_{i,j,k}) = \text{clip} \left(\left\lfloor \frac{K_{i,j,k} - Z_{i,j,g}}{S_{i,j,g}} \right\rfloor, 0, 2^b - 1 \right) \quad (10)$$

where $\lfloor \cdot \rfloor$ is the round-to-nearest function and $g = \lfloor \frac{k-1}{G} \rfloor + 1$ is the group index of $K_{i,j,k}$. The corresponding zero point is computed as $Z_{i,j,g} = \min(\mathcal{G}_{i,j,g})$ and its scale factor as

$$S_{i,j,g} = \frac{\max(\mathcal{G}_{i,j,g}) - Z_{i,j,g}}{2^b - 1} \quad (11)$$

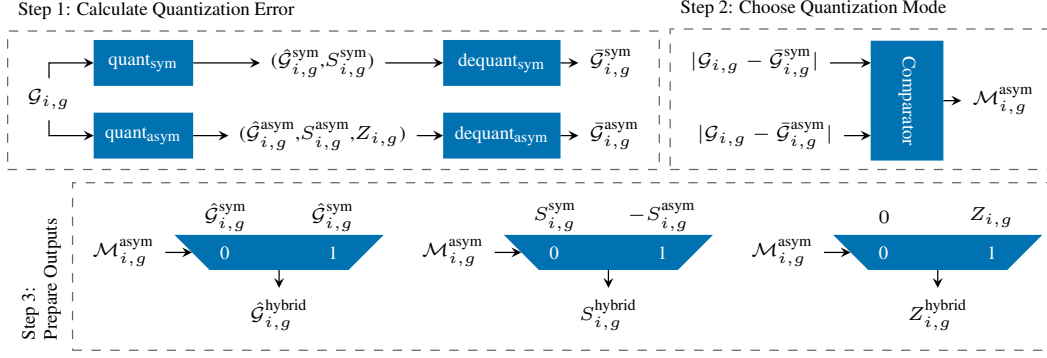


Figure 3: High-level view of the quantization process in the hybrid quantization mode for a quantization group $\mathcal{G}_{i,g}$.

where $\mathcal{G}_{i,j,g} = \{K_{i,j,k} \mid \lfloor (k-1)/G \rfloor = g\}$ is the set of values in the group. As the values are shifted by their minimum, for all i, j , and k we have $0 \leq \hat{K}_{i,j,k}$ and thus \hat{K} is represented with an unsigned data type. Similarly, $\hat{K}_{i,j,k}$ is dequantized as

$$\text{dequant}_{\text{asym}}(\hat{K}_{i,j,k}) = S_{i,j,g} \hat{K}_{i,j,k} + Z_{i,j,g}. \quad (12)$$

Symmetric quantization is equivalent to asymmetric quantization, except that the zero-point is fixed to 0 for all groups. Accordingly, the quantization and dequantization processes follow Equations (10) and (12) with $Z_{i,j,g} = 0$. The scale factor for each group is then computed using the maximum absolute value as

$$S_{i,j,g} = \frac{\max(|\mathcal{G}_{i,j,g}|)}{2^b - 1} \quad (13)$$

where $|\cdot|$ is the absolute value operator. Here, unlike asymmetric quantization, quantized values can be either negative or positive and are represented using signed data types.

4.1.2 Hybrid Quantization

As their names suggest, symmetric and asymmetric quantization impose different assumptions on the data distribution. The extent to which these assumptions are satisfied directly influences the fidelity of the quantized representation. To illustrate, consider a quantization group \mathcal{G} such that $\min(\mathcal{G}) > 0$. Symmetric quantization allocates a sign bit to represent the quantized values in \mathcal{G} . For an entirely positive group, this reduces effective resolution by reserving part of the range for values that never occur. In contrast, asymmetric quantization exploits the nonnegativity of \mathcal{G} by shifting the quantization interval, thereby using the available bit budget more efficiently to represent magnitudes rather than an unused negative range.

Empirically, the distribution of activation and weight values varies substantially across models and layers (see Figure 2 in [14]). This variation suggests that the preferable choice between symmetric and asymmetric quantization is configuration-dependent rather than universal. Consistent with this observation, our ablation results in Section 6.3 show that model performance can be sensitive to the quantization mode.

To address this sensitivity, we propose a *hybrid quantization* scheme in which each quantization group independently selects between symmetric and asymmetric quantization. Following the notation of Section 4.1.1, we introduce a binary mask $\mathcal{M} \in \{0, 1\}^{n_h \times N_K \times \frac{d_h}{G}}$, where $\mathcal{M}_{i,j,g} = 1$ indicates that $\mathcal{G}_{i,j,g}$ is quantized using the asymmetric mode, and $\mathcal{M}_{i,j,g} = 0$ indicates that it is quantized using the symmetric mode. As depicted in Figure 3, we determine $\mathcal{M}_{i,j,g}$ by finding the quantization mode with the lower reconstruction error.

Following the notation of Section 4.1.1, we have

$$\text{dequant}_{\text{hybrid}}(\hat{K}_{i,j,k}) = S_{i,j,g} \hat{K}_{i,j,k} + \mathcal{M}_{i,j,g} Z_{i,j,g}. \quad (14)$$

When $\mathcal{M}_{i,j,g} = 0$, the zero-point term does not contribute to dequantization. Although our experiments reveal that hybrid quantization rarely uses asymmetric quantization for groups, we store the zero-points as a dense matrix to avoid the latency overhead associated with sparse representations. We study the sparsity of \mathcal{M} and its impact on the latency of dequantization operations in Section 6.2. Since scale factors are strictly positive, we repurpose their sign bit to encode $\mathcal{M}_{i,j,g}$. We further discuss the hardware-aware implementation of the hybrid quantization mode in Section 5.3.

4.2 High-precision Window

As shown in previous work, keeping a small window of KV cache tokens in a high-precision data type greatly helps maintain model accuracy [14, 5, 22, 20]. We keep the last w_{recent} tokens in half-precision and denote them as K_{recent} and V_{recent} . Similarly, the first w_{sink} tokens are also kept in half-precision and are referred to as K_{sink} and V_{sink} . Given that finding the exact tokens that act as attention sinks appear incurs additional computational overhead [17, 22], we set a fixed w_{sink} for all setups. We study the effect of changing w_{sink} and w_{recent} in Section 6.1.

Incorporating the high-precision windows into Equation (8), we have

$$\begin{aligned} K_{\text{sink}} &= K_{:,w_{\text{sink}}:,} & V_{\text{sink}} &= V_{:,w_{\text{sink}}:,} \\ K_{\text{recent}} &= K_{:,-w_{\text{recent}}:,} & V_{\text{recent}} &= V_{:,-w_{\text{recent}}:,} \\ \hat{K}_{\text{cache}} &= \text{quant}(K_{:,w_{\text{sink}}:-w_{\text{recent}}:,}) & \hat{V}_{\text{cache}} &= \text{quant}(V_{:,w_{\text{sink}}:-w_{\text{recent}}:,}). \end{aligned} \quad (15)$$

During the decode phase, K_{sink} and V_{sink} remain fixed, while the newly generated K and V for each token are appended to K_{recent} and V_{recent} . As tokens accumulate in K_{recent} and V_{recent} , the oldest ones are quantized and moved to \hat{K}_{cache} and \hat{V}_{cache} . While in per-channel group-wise quantization the old tokens can be quantized one by one, per-token group-wise quantization requires the number of quantized tokens to be a multiple of the group size.

4.3 Per-channel Normalization of K

Outliers within a quantization group reduce the effective precision available to the remaining values. Prior work has shown that such outliers emerge along the channel dimension of K [14]. To mitigate this effect, we apply per-channel normalization to K which is beneficial in mitigating outliers when quantization groups span multiple channels, as in per-token group-wise quantization (our work). Specifically, the normalization factor for channel k is defined as $\text{norm}_k^K = \sqrt{\max(|K_{:,k}|)}$, where $|\cdot|$ denotes the absolute value. The vector norm^K is computed once at the end of the prefill stage and absorbed into W_Q and W_K , thereby hiding the normalization overhead during decoding.

4.4 InnerQ: Quantizing Key and Value Over the Inner Dimension

At each step of the decode phase, quantized KV cache matrices are dequantized and then used by Equations (3) and (5) to compute the output. Since $N_Q = 1$ in the decode stage, Equations (3) and (5) are implemented as vector-matrix multiplication operations (GEMV). Given the high latency of memory operations in modern GPU hardware, it is suboptimal to perform the dequantization and GEMV operations separately. Instead, as suggested by previous work [14], these operations are performed in a fused kernel where each row of the quantized matrix is dequantized and then multiplied by the floating-point vector. The fused kernel allows the output of the dequantization operation to directly pass to the GEMV operation without using the high-latency global memory to store the intermediate results.

We propose to align the quantization groups with the dimension over which the multiplication is performed, i.e. the *inner* dimension. As depicted in Figure 1b, when grouped over the inner dimension, values of the same group in each channel of K have the same scale factor². This enables compute units processing the same channel group to load the scale factor once and reuse it. In contrast, outer dimension quantization, where grouping is done over the tokens, loads multiple scale factors per row. In this scheme, compute units do not reuse these values and each loads its own scale factor which leads to multiple repeated high-bandwidth memory loads. As a result of the aligned

²A similar argument is valid for zero-points in the case of asymmetric quantization.

memory access patterns, inner grouping can achieve a higher throughput and improve the overall latency of the attention operation. The effect of aligned memory access is even more pronounced in edge devices where memory bandwidth and cache size are limited. A similar argument is valid for Equation (5) where P is a floating-point vector and V is a quantized matrix in which the token dimension is the inner dimension and the channel dimension is the outer dimension. In Section 5.3, we validate this hypothesis by comparing the latency of quantized GEMV kernels under inner- and outer-dimension grouping.

We present **InnerQ**, a hardware-aware KV cache quantization method designed to reduce the latency of large language model inference during the decode phase. We introduce three variants of InnerQ to allow a tunable trade-off between numerical precision, inference latency, and memory footprint. The variants differ primarily in how they quantize V_{cache} , while sharing the same strategy for K_{cache} . We first describe the quantization scheme shared by all variants and then summarize the variant-specific choices for V_{cache} quantization.

All variants apply inner dimension grouping to both key and value matrices. Specifically, K_{cache} is quantized using per-token group-wise quantization, and V_{cache} is quantized using per-channel group-wise quantization. For K_{cache} , we use 3-bit symmetric quantization in all variants; thus each $\hat{K}_{i,j,k}$ is represented as a 3-bit signed integer. Consistent with Section 4.2, we maintain high-precision windows for recent and sink tokens. We also apply per-channel normalization to K following Section 4.3 to reduce sensitivity to outliers.

InnerQ_{Base} quantizes V_{cache} using 3-bit symmetric quantization. Based on the observation that V_{cache} has a higher tolerance for quantization [8], **InnerQ_{Small}** applies 2-bit symmetric quantization to V_{cache} and reduces bandwidth and latency, at the expense of reduced dynamic range. To compensate for this limitation, **InnerQ_{Hybrid}** adopts 2-bit hybrid quantization (Section 4.1.2) for V_{cache} , achieving higher fidelity at a modest storage and runtime cost relative to InnerQ_{Small}.

5 Empirical Evaluation

5.1 Evaluation Metric Score

We apply InnerQ to Llama [19, 7] and Mistral [10] language models and observe its effect on the metric score of the model. We implement a simulated quantized KV cache based on the Hugging Face Transformers library [21] and use the LM-eval [6] framework to build our evaluation script. We compare our results against non-quantized FP16 KV cache as the baseline. We also compare our work with KIVI [14] as a tuning-free KV cache quantization method that uses group-wise quantization. For a better comparison, we provide an additional setup denoted as KIVI_{Sink} by following Section 4.2 and devoting a portion of the high-precision window to the sink tokens. Following previous work we set the group size to 32 and the total length of the high-precision window to 128. For KIVI_{Sink} and InnerQ we have $w_{\text{sink}} = 32$ and $w_{\text{recent}} = 96$ and for KIVI we have $w_{\text{sink}} = 0$ and $w_{\text{recent}} = 128$. In addition to KIVI, we run evaluation experiments while quantizing the KV cache with the recently proposed TurboQuant method [23]. As our experiments and models use softmax-based attention, we use the MSE variant of TurboQuant with a high-precision window size of 128. We also set the key bit-width and value bit-width of TurboQuant to 4 and 3, respectively, which makes it comparable in size to InnerQ_{Base} (Table 3). For KIVI and InnerQ we use our own quantized KV cache implementation while for TurboQuant we use a community implementation [18].

We compare the performance of InnerQ with other setups by applying them to pre-trained models and running few-shot evaluation on the evaluation set of mathematical reasoning tasks GSM8K [4] and Minerva Math [12]. We also use the instruction-tuned variants of the language models and run evaluation experiments on few-shot code-generation tasks HumanEval [3] and MBPP [1].

Our experimental results in Table 1 identify InnerQ_{Base} as the most accurate variant of our method. On average, it improves the score of KIVI and KIVI_{Sink} by 1.8 and 3.5 points, respectively. InnerQ_{Base} also achieves an average gain of 0.4 points over TurboQuant. A more fine-grained analysis shows that InnerQ_{Base} has a higher average score than TurboQuant on GSM8K, HumanEval, and MBPP tasks.

Among the InnerQ variants, InnerQ_{Small} exhibits an average degradation of 3 points relative to InnerQ_{Base}, which can be attributed to its 2-bit value cache. In contrast, the hybrid quantization

Dataset	Model	Baseline	KIVI	KIVISink	TurboQuant	InnerQBase	InnerQHybrid	InnerQSmall
GSM8k	Llama 3.2-1B	6.22	2.81	4.02	5.84	5.53	5.31	4.63
	Llama 3.2-3B	26.46	19.33	23.35	25.47	27.14	23.12	24.03
	Llama 3.1-8B	49.96	42.84	47.84	48.90	48.22	47.31	45.94
	Llama 2-7B	13.04	13.12	11.90	12.59	13.42	11.30	0.46
	Mistral 7B v0.3	36.92	32.30	33.81	34.72	36.47	33.89	33.89
	Average	26.52	22.08	24.18	25.50	26.16	24.19	21.79
Minerva Math (500)	Llama 3.2-1B	4.40	5.20	3.80	3.60	3.40	3.40	2.80
	Llama 3.2-3B	9.20	6.80	8.60	11.40	10.80	8.40	6.60
	Llama 3.1-8B	21.60	17.20	21.00	21.20	20.80	19.60	19.00
	Llama 2-7B	3.20	3.60	4.00	5.20	3.00	3.40	0.40
	Mistral 7B v0.3	11.60	10.40	10.40	12.80	12.60	11.40	9.80
	Average	10.00	8.64	9.56	10.84	10.12	9.24	7.72
HumanEval	Llama 3.2-1B	33.54	21.34	33.54	32.72	34.15	27.44	28.66
	Llama 3.2-3B	52.44	52.44	53.05	56.71	52.44	53.66	53.05
	Llama 3.1-8B	67.07	64.02	64.02	63.42	66.46	64.63	64.63
	Mistral 7B v0.3	40.85	41.46	36.59	41.46	44.51	40.85	39.02
		Average	48.47	44.81	46.80	48.58	49.39	46.64
MBPP	Llama 3.2-1B	37.00	26.20	34.00	34.20	37.80	35.00	34.20
	Llama 3.2-3B	51.60	49.40	49.40	49.60	50.00	49.40	49.20
	Llama 3.1-8B	60.00	57.20	58.40	59.80	59.40	59.80	59.00
	Mistral 7B v0.3	42.60	40.40	39.20	42.60	42.40	39.80	38.80
		Average	47.80	43.30	45.25	46.55	47.40	46.00

Table 1: Evaluation metric score of models on different language generation tasks with quantized KV cache, compared to the non-quantized FP16 baseline. We report `flexible_extract` for GSM8k, `math_verify` for Minerva Math, and `pass_at_1` for Humaneval and MBPP tasks. We use instruction-tuned models for the Humaneval and MBPP tasks.

strategy used in InnerQHybrid reduces the average gap to InnerQBase to 1.7 points, while achieving an average score comparable to KIVISink.

A secondary observation from Table 1 is the performance gap between KIVI and KIVISink. This gap indicates that introducing a high-precision sink window into KIVI has a substantial effect on performance, increasing the average score of KIVISink by 1.7 points over KIVI. We investigate the effect of the high-precision window size in Section 6.1.

We further evaluate the proposed KV cache quantization methods in long-sequence generation settings using selected tasks from the LongBench benchmark [2]. The results, reported in Table 2, indicate that the benefit of the high-precision sink window diminishes as the sequence length increases. In several cases, KIVI outperforms KIVISink; on average, KIVISink improves over KIVI by only 0.2 points. InnerQBase remains competitive with existing KV cache quantization methods, improving the average score over KIVI and KIVISink by 0.4 and 0.2 points, respectively.

Consistent with the results in Table 1, InnerQSmall incurs an average degradation of 4.3 points relative to InnerQBase, further highlighting the sensitivity of model performance to aggressive value-cache quantization. Similar to results on the shorter-context benchmarks, InnerQHybrid recovers a substantial portion of the performance loss introduced by low-bit value-cache quantization. On average, InnerQHybrid lags behind InnerQBase by only 0.5 points while outperforming InnerQSmall by 3.8 points. The performance of InnerQHybrid across the tasks reported in Tables 1 and 2 demonstrates the effectiveness of hybrid quantization for adapting value-cache quantization in low-bit regimes.

Overall, the experimental results indicate that InnerQBase matches or surpasses existing KV cache quantization methods in evaluation metric score. As shown in Section 5.3, InnerQBase also reduces the latency associated with using the quantized KV cache relative to both KIVI and TurboQuant. Taken together, the metric and latency results further demonstrate the effectiveness of InnerQHybrid, which preserves comparable metric score while maintaining low latency.

5.2 Bit-width

Table 3 summarizes the total effective bit-width of various KV cache quantization methods, including both the base integer bit-width and the overhead of scale factors, zero-points, and channel norms. With a group size of 32 for KIVI and InnerQ, storing an FP16 scale factor (zero-point) contributes

Dataset	Model	Baseline	KIVI	KIVISink	InnerQBase	InnerQHybrid	InnerQSmall
gasper	Llama 3.2-1B	20.29	18.00	17.23	18.37	20.43	19.84
	Llama 3.2-3B	40.63	37.09	38.49	40.32	39.59	38.84
	Llama 3.1-8B	44.58	44.08	43.61	44.59	42.40	42.36
	Llama 2-7B	20.99	21.11	20.30	21.84	22.18	13.12
	Llama 2-13B	16.59	15.09	15.48	17.85	16.56	17.50
gov-report	Llama 3.2-1B	29.27	28.57	28.87	28.89	26.72	26.70
	Llama 3.2-3B	33.86	32.11	33.76	33.38	32.73	32.25
	Llama 3.1-8B	34.61	34.47	34.33	34.33	33.62	33.80
	Llama 2-7B	26.88	26.68	26.64	26.12	25.18	17.15
	Llama 2-13B	27.82	27.01	27.10	27.29	26.38	25.69
multinews	Llama 3.2-1B	26.08	25.89	26.02	26.07	25.06	24.70
	Llama 3.2-3B	25.93	25.74	26.07	25.70	25.43	25.35
	Llama 3.1-8B	26.95	26.39	26.76	26.73	26.20	26.09
	Llama 2-7B	26.17	25.93	25.8	25.80	26.18	11.7
	Llama 2-13B	26.56	25.78	26.26	26.17	25.97	26.16
trec	Llama 3.2-1B	2.00	2.75	3.50	4.75	4.50	3.50
	Llama 3.2-3B	10.03	8.53	9.03	10.50	8.10	9.10
	Llama 3.1-8B	39.50	32.50	34.50	37.00	37.50	38.00
	Llama 2-7B	64.00	64.50	64.50	64.50	64.50	62.00
	Llama 2-13B	68.50	68.00	68.00	67.50	67.50	66.50
triviaqa	Llama 3.2-1B	64.03	63.92	64.75	62.92	59.06	59.20
	Llama 3.2-3B	69.39	67.29	67.53	67.48	65.37	65.41
	Llama 3.1-8B	91.64	90.53	91.33	91.51	91.70	91.70
	Llama 2-7B	83.51	82.77	82.27	83.84	83.32	39.51
	Llama 2-13B	87.85	87.97	87.83	87.47	88.27	84.55
samsum	Llama 3.2-1B	6.04	6.83	6.11	6.57	6.18	6.25
	Llama 3.2-3B	6.70	7.16	7.48	7.00	7.06	7.13
	Llama 3.1-8B	43.57	42.33	43.09	43.38	42.82	43.12
	Llama 2-7B	41.36	40.37	40.44	40.62	40.16	14.77
	Llama 2-13B	42.55	42.12	42.57	42.16	41.77	40.54
lcc	Llama 3.2-1B	19.29	19.17	18.70	18.29	18.15	18.53
	Llama 3.2-3B	31.65	31.27	31.01	30.20	30.98	31.63
	Llama 3.1-8B	43.02	42.85	42.66	42.97	42.76	42.84
	Llama 2-7B	58.29	57.79	58.12	58.41	57.80	40.41
	Llama 2-13B	48.22	47.31	48.51	48.04	49.50	46.45
repobench-p	Llama 3.2-1B	16.61	17.33	15.41	14.54	14.43	15.84
	Llama 3.2-3B	29.56	29.36	29.44	29.19	29.02	29.34
	Llama 3.1-8B	38.26	38.21	38.37	38.23	38.08	37.93
	Llama 2-7B	52.05	51.57	52.04	52.03	50.43	28.71
	Llama 2-13B	49.78	48.59	49.03	49.71	49.05	46.14

Table 2: Evaluation metric score of models on select tasks from the longbench suite with quantized KV cache, compared to the non-quantized FP16 baseline. We report F1 for gasper and triviaqa, ROUGE-L for gov-report, multinews, and samsum, accuracy for trec, and pass_at_1 for repobench-p. We use instruction-tuned models for Llama 3 models and chat version of Llama 2 models.

$\frac{16}{32} = 0.5$ additional bits per quantized number. Although the zero-point matrix in InnerQHybrid is highly sparse, we still budget 0.5 bits for the zero-point overhead and defer exploiting sparsity to future work. To measure the overhead of storing channel norms for TurboQuant, we assume a head dimension of 128 and FP32 channel norms, which leads to 0.25 bits of overhead per quantized number.

5.3 Latency

We evaluate how different KV cache quantization methods affect the latency of token generation in the decode phase. To this end, we implement fused CUDA kernels that perform dequantization and GEMV on their input. The fused kernel takes a quantized matrix and an FP16 vector to simulate

		KIVI	TurboQuant	InnerQ _{Base}	InnerQ _{Hybrid}	InnerQ _{Small}
Key Cache	Integer Bit-width	2	4	3	3	3
	Scale Factor Overhead	0.5	–	0.5	0.5	0.5
	Zero-point Overhead	0.5	–	–	–	–
	Channel Norm Overhead	–	0.25	–	–	–
Value Cache	Integer Bit-width	2	3	3	2	2
	Scale Factor Overhead	0.5	–	0.5	0.5	0.5
	Zero-point Overhead	0.5	–	–	0.5	–
	Channel Norm Overhead	–	0.25	–	–	–
Per-number Effective Bit-width		3	3.75	3.5	3.25	3

Table 3: The per-number effective bit-width of different KV cache quantization methods. Bits for scale factors and zero-points are averaged to represent the overhead on each quantized number. We assume that scale factors and zero-points are represented using FP16 while channel norms are represented using FP32. The group size is 32 and the head dimension is 128.

Method		Sequence Length						
		512	1024	2048	4096	8192	16384	32768
Key Cache (Equation (3))	Baseline (FP16)	76	147	291	576	1148	2291	4593
	KIVI	39	72	138	270	535	1063	2120
	TurboQuant	34	62	118	230	453	901	1796
	InnerQ _{Base}	30	53	99	192	378	749	1492
	InnerQ _{Hybrid}	30	53	99	192	378	749	1492
	InnerQ _{Small}	30	53	99	192	378	749	1492
Value Cache (Equation (5))	Baseline (FP16)	76	148	291	597	1172	2347	4922
	KIVI	40	73	139	273	538	1079	2210
	TurboQuant	40	78	149	286	563	1126	2250
	InnerQ _{Base}	34	65	120	228	443	883	1784
	InnerQ _{Hybrid}	33	59	110	214	423	842	1688
	InnerQ _{Small}	32	57	109	211	416	826	1644
Total	Baseline (FP16)	153	295	582	1174	2320	4638	9516
	KIVI	79	146	278	543	1074	2142	4331
	TurboQuant	75	140	267	516	1017	2027	4046
	InnerQ _{Base}	64	118	220	420	822	1633	3276
	InnerQ _{Hybrid}	63	112	210	406	801	1591	3180
	InnerQ _{Small}	62	110	208	403	795	1575	3136

Table 4: Latency breakdown (μ s) of the fused dequantize-GEMV kernels for Llama 3.1-8B using different KV cache quantization methods along with the FP16 GEMV as the baseline.

Equations (3) and (5) in the decode phase with a quantized KV cache. We set the batch size to 1 to reflect the interactive usage of an end-user generating text on an edge device. We run our latency measurements on the NVIDIA Jetson Xavier NX embedded platform. Reported latencies (in microseconds) are collected after 10 warm-up iterations and are averaged over 100 measured runs. Table 4 reports the latency of Equations (3) and (5) using quantized key and value caches for one layer of Llama 3.2-8B across different sequence lengths. We assume that for the value cache in InnerQ_{Hybrid} \mathcal{M} is 99% sparse. Figure 4 summarizes these measurements by plotting the speedup of each InnerQ variant over the FP16 baseline, KIVI, and TurboQuant.

As discussed in Section 4.4, the proposed InnerQ variants differ mainly in their quantization policy for the value cache. Our experiments show that InnerQ_{Small} achieves the lowest latency due to its lower bit-width. InnerQ_{Hybrid} is slightly slower due to its higher computational demand and the need to load additional zero-points for some groups. We further study the impact of the level of sparsity of \mathcal{M} in the hybrid quantization scheme on the latency of the fused kernel in Section 6.2. As shown in the leftmost part of Figure 4, all InnerQ variants achieve a comparable average speedup of $2.7\times$ relative to the FP16 baseline which steadily rises as the sequence length grows.

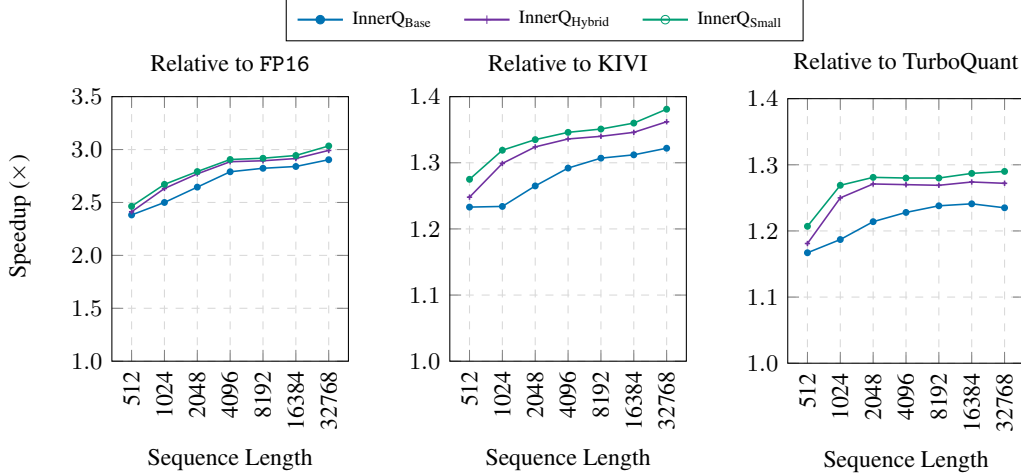


Figure 4: Total speedup in the operations in Llama 3.1-8B associated with KV cache when using InnerQ variants for KV cache quantization, relative to (left) non-quantized FP16, (middle) KIVI [14], and (right) TurboQuant [23].

	KIVI	TurboQuant	InnerQ _{Base}	InnerQ _{Hybrid}	InnerQ _{Small}
Key Cache	1.0	15.9	17.3	17.3	17.3
Value Cache	21.1	16.1	1.0	1.4	0.9
Total	22.1	31.9	18.3	18.7	18.2

Table 5: Latency breakdown (μ s) of the quantization operations during the decode phase for Llama 3.1-8B using different quantization methods.

Compared with KIVI, all InnerQ variants are notably faster and achieve consistently lower latency across different sequence lengths. The speedup of InnerQ_{Base} and InnerQ_{Hybrid} relative to KIVI exceeds $1.2\times$ despite their average bit-widths being higher than KIVI. This highlights the importance of data reuse and its potential to reduce the latency of quantized KV cache operations. As the sequence length grows, the latency gap between KIVI and InnerQ variants widens in favor of InnerQ. Notably, when 32768 tokens are stored in the KV cache, the relative speedup of InnerQ_{Small} compared to KIVI is nearly $1.4\times$.

TurboQuant employs a precomputed codebook for dequantization, along with online per-channel normalization to rescale the dequantized key and value matrices to their original range. We omit the normalization step for the value cache and assume that its contribution to the latency is negligible as it can be fused into the softmax operation. Although TurboQuant requires fewer normalization factors than the scaling factors used in InnerQ, the codebook lookup requires multiple accesses to CUDA shared memory, thereby increasing kernel latency. As illustrated in Figure 4, InnerQ_{Base} achieves a relatively consistent $1.2\times$ speedup over TurboQuant. Other InnerQ variants further improve the speedup to approximately $1.3\times$, at the expense of a reduction in evaluation performance as detailed in Section 5.1.

Beyond the fused dequantization and GEMV kernels, we also develop CUDA kernels to handle quantization for each method. As noted in Section 4.2, tokens evicted from the high-precision windows K_{recent} and V_{recent} are quantized and stored in \hat{K}_{cache} and \hat{V}_{cache} . The eviction pattern is governed by the dimension across which quantization groups are defined in the cache. InnerQ employs per-token group-wise quantization for the key cache and per-channel group-wise quantization for the value cache, whereas KIVI uses per-channel quantization for keys and per-token quantization for values. This design leads InnerQ to quantize one key token at every step, while value tokens are evicted and quantized in groups of G (32) every 32 steps. Conversely, KIVI evicts and quantizes 32 key tokens every 32 steps and one value token at each step. Unlike KIVI and InnerQ, which are group-wise quantization methods, TurboQuant quantizes one key and one value token at each step.

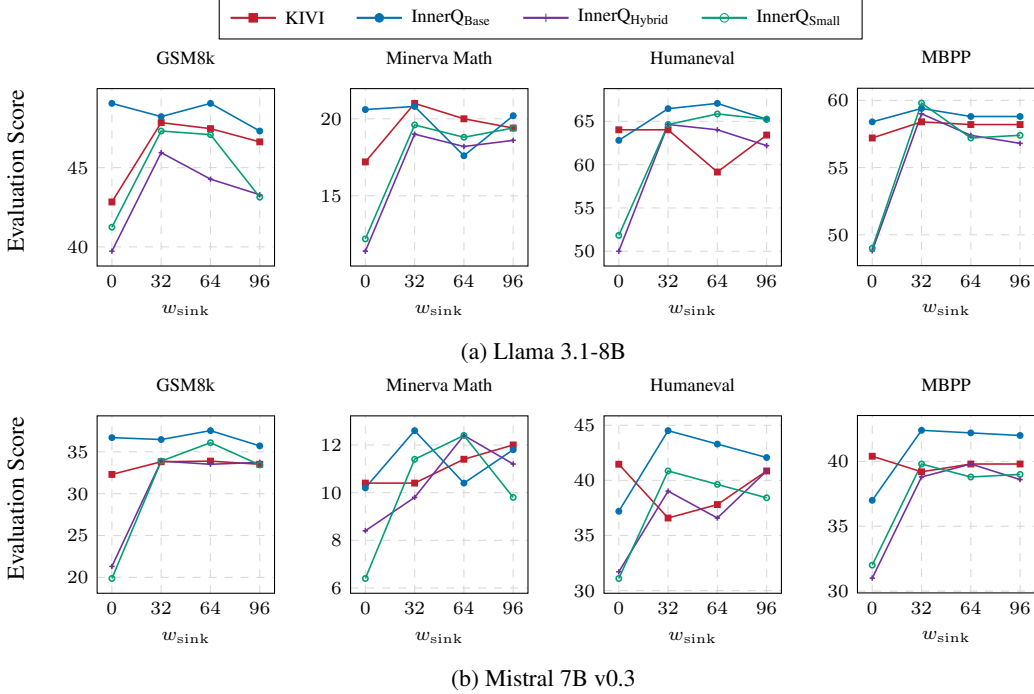


Figure 5: Effect of changing w_{sink} on the evaluation metric performance of (a) Llama 3.1-8B and (b) Mistral 7B v0.3. At each step $w_{\text{recent}} = 128 - w_{\text{sink}}$. We report `flexible_extract` for GSM8k, `math_verify` for Minerva Math, and `pass_at_1` for Humaneval and MBPP tasks. We use instruct tuned models for the Humaneval and MBPP tasks.

Based on their eviction behavior, we measure and report the average quantization latency overhead during the decode phase. As shown in Table 5, the latency gap between KIVI and InnerQ is marginal, amounting to approximately $2 \mu\text{s}$. Because TurboQuant performs quantization more frequently, it incurs a higher quantization overhead. Considering the latencies reported in Table 4, this additional $14 \mu\text{s}$ overhead can reduce the overall throughput of TurboQuant, particularly for small- to medium-length sequences. Unlike dequantization, which lies on the critical path for producing the attention output, quantization of newly evicted tokens from K_{recent} and V_{recent} does not directly impact output generation. This property provides an opportunity to pipeline the quantization process during periods of GPU idleness and mask its latency. We leave the design and evaluation of such pipelining strategies to future work.

6 Ablation Studies

6.1 High-precision Window Size

To analyze the effect of high-precision windows on models with quantized KV caches, we vary the hyperparameters w_{sink} and w_{recent} . We maintain a fixed number of total high-precision tokens by adjusting w_{sink} and setting $w_{\text{recent}} = 128 - w_{\text{sink}}$.

Figure 5 illustrates the evaluation performance of different models across window configurations and tasks. Our findings reveal that the impact of window size on performance is highly dependent on both the model and the task. Nonetheless, in many cases, allocating even a modest high-precision window of size 32 yields a substantial accuracy improvement. This behavior is especially pronounced for KIVI, InnerQHybrid, and InnerQSmall, whereas InnerQBase demonstrates stable performance even when no high-precision sink window is used.

We also observe that in certain scenarios, such as GSM8K on Mistral 7B v0.3, further increasing w_{sink} at the expense of w_{recent} has a negligible effect on the metric score. In contrast, other scenarios show a clear performance optimum, underscoring the importance of balancing the sizes of the two

Sparsity of \mathcal{M}	Sequence Length			
	1024	4096	16384	32768
99%	59.0	214.4	841.9	1685.4
90%	61.2	218.6	849.0	1701.5
50%	65.3	231.2	900.1	1800.7
1%	65.9	233.1	910.1	1814.9

Table 6: Latency (μ s) of the fused hybrid dequantization and GEMV in Llama 3.1-8B for Equation (5) for different cache sizes and levels of sparsity of \mathcal{M} .

Bit-width	Quantization Mode	Model			
		Llama 3.2-3B	Llama 3.1-8B	Llama 2-7B	Mistral 7B v0.3
$K:3, V:3$	$K:\text{Sym}, V:\text{Sym}$	27.14	48.22	13.42	36.47
	$K:\text{Sym}, V:\text{Asym}$	25.78	48.67	12.66	35.86
	$K:\text{Asym}, V:\text{Sym}$	25.17	48.60	13.27	36.39
	$K:\text{Asym}, V:\text{Asym}$	23.88	47.23	12.13	32.37
	$K:\text{Sym}, V:\text{Hybrid}$	27.29	48.60	13.27	37.60
$K:3, V:2$	$K:\text{Sym}, V:\text{Sym}$	24.03	45.94	0.45	33.89
	$K:\text{Sym}, V:\text{Asym}$	14.03	36.69	3.41	2.05
	$K:\text{Asym}, V:\text{Sym}$	21.76	44.05	0.68	33.36
	$K:\text{Asym}, V:\text{Asym}$	10.31	30.93	2.50	1.67
	$K:\text{Sym}, V:\text{Hybrid}$	23.12	47.31	11.30	33.89

Table 7: `flexible_extract` evaluation score on GSM8K for different KV-cache quantization modes across four language models. In all configurations, both K and V are quantized along their inner dimensions.

windows. We defer a systematic investigation of optimal window sizes and the selection of tokens included in each window to future work.

6.2 Sparsity of \mathcal{M}

Section 4.1.2 defines \mathcal{M} as a binary mask that determines the quantization method assigned to each group. To analyze its behavior, we randomly sample 50 instances from the evaluation set of each task and record \mathcal{M} for all layers. Across tasks and models, \mathcal{M} has an average sparsity of 99%. The only exception is Llama 3.2-1B on Minerva Math, where the average sparsity drops to 90%. Overall, these observations suggest that hybrid quantization overwhelmingly favors symmetric quantization across quantization groups. However, as reported in Table 1, this seemingly slight difference in the quantization mode results in an average 1.3 score improvement for $\text{InnerQ}_{\text{Hybrid}}$ over $\text{InnerQ}_{\text{Small}}$.

We also ablate the sparsity of \mathcal{M} and observe its impact on the latency of the fused dequantization kernel. Comparing the value cache latencies in Table 6 with the reported latencies in Table 4 shows that reducing the sparsity from 99% to 90% slightly increases the latency of the fused kernel. Further reducing the sparsity increases this latency to levels higher than the latency of $\text{InnerQ}_{\text{Base}}$. However, even at the lowest sparsity, the latency of $\text{InnerQ}_{\text{Hybrid}}$ is still lower than both TurboQuant and KIVI.

6.3 Quantization Mode

We study the effect of varying the KV cache quantization mode on model evaluation performance. We change the quantization mode of the key and value cache matrices between symmetric and asymmetric forms and report the results in Table 7.

While we observe an overall decreasing trend in the model score when using asymmetric quantization, the extent of the score drop depends on the model and the setup. When both the key and value caches are quantized to 3 bits, the effect of the quantization mode is more limited. For example, for Llama 3.1-8B, a noticeable reduction appears only when both K and V are quantized asymmetrically, while for Llama 3.2-3B the model score drops as soon as either K or V is changed to asymmetric mode. In

contrast, when the V bit-width is reduced to 2 bits, switching to asymmetric quantization has a larger impact on the evaluation score across all models.

The last row in each bit-width group applies hybrid quantization to V to address the above-mentioned sensitivity of the KV cache to the quantization mode. Hybrid quantization adjusts the quantization mode per-group according to each group’s underlying data distributions. The results show that this approach largely recovers the score reduction associated with asymmetric quantization and, in some cases, exceeds the best non-hybrid configuration. This effect is more pronounced when the value cache is quantized to 2 bits. For instance, in Llama 2-7B, the configuration with hybrid quantization for the value cache is the only one that maintains a non-trivial score, whereas the remaining configurations yield near-zero results.

Taken together, the results in Table 7 indicate that the choice of quantization mode significantly affects evaluation performance, and that the adaptive hybrid quantization provides an effective mechanism for preserving performance under low-bit KV cache quantization.

7 Conclusion

In this work, we introduced InnerQ, a hardware-aware KV cache quantization scheme that achieves an average speedup of $1.3\times$ over existing KV cache quantization methods and $2.7\times$ over the non-quantized cache. This improvement is enabled by applying group-wise quantization with groups formed along the inner dimension of the quantized matrices. By aligning the quantization layout with the execution flow of vector-matrix multiplication, InnerQ reduces memory traffic and dequantization overhead.

To preserve evaluation performance, InnerQ combines this hardware-friendly layout with high-precision windows for both recent tokens and early attention sinks, together with per-channel normalization of the key cache. We introduced three InnerQ variants that offer different trade-offs between evaluation performance and inference latency: InnerQ_{Base}, InnerQ_{Hybrid}, and InnerQ_{Small}. InnerQ_{Base} prioritizes metric score, InnerQ_{Small} emphasizes latency reduction, and InnerQ_{Hybrid} provides an intermediate trade-off.

Our results show that all InnerQ variants improve inference speed over prior KV cache quantization methods. In particular, InnerQ_{Base} achieves evaluation performance comparable to strong existing methods such as TurboQuant [23] and KIVI [14], while reducing KV cache latency. The results further demonstrate the effectiveness of our proposed hybrid quantization strategy used in InnerQ_{Hybrid}, which maintains competitive evaluation scores despite the low bit-width value cache.

Overall, InnerQ demonstrates that KV cache quantization can benefit substantially from co-designing numerical representation with hardware memory-access patterns. These results highlight the importance of hardware-aware quantization layouts for maximizing efficiency gains in long-context large language model inference.

Future work will systematically examine how our quantization scheme interacts with alternative KV cache eviction strategies. Another direction is to design adaptive and low-overhead policies for selecting tokens that are retained in the high-precision windows.

References

- [1] J. Austin, A. Odena, M. Nye, M. Bosma, H. Michalewski, D. Dohan, E. Jiang, C. Cai, M. Terry, Q. Le, et al. Program synthesis with large language models. *arXiv preprint arXiv:2108.07732*, 2021. doi: 10.48550/arXiv.2108.07732.
- [2] Y. Bai, X. Lv, J. Zhang, H. Lyu, J. Tang, Z. Huang, Z. Du, X. Liu, A. Zeng, L. Hou, Y. Dong, J. Tang, and J. Li. LongBench: A bilingual, multitask benchmark for long context understanding. In *Proceedings of the 62nd Annual Meeting of the Association for Computational Linguistics (Volume 1: Long Papers)*, pages 3119–3137, Bangkok, Thailand, Aug. 2024. Association for Computational Linguistics. doi: 10.18653/v1/2024.acl-long.172. URL <https://aclanthology.org/2024.acl-long.172>.
- [3] M. Chen, J. Tworek, H. Jun, Q. Yuan, H. P. de Oliveira Pinto, J. Kaplan, H. Edwards, Y. Burda, N. Joseph, G. Brockman, A. Ray, R. Puri, G. Krueger, M. Petrov, H. Khlaaf, G. Sastry,

- P. Mishkin, B. Chan, S. Gray, N. Ryder, M. Pavlov, A. Power, L. Kaiser, M. Bavarian, C. Winter, P. Tillet, F. P. Such, D. Cummings, M. Plappert, F. Chantzis, E. Barnes, A. Herbert-Voss, W. H. Guss, A. Nichol, A. Paino, N. Tezak, J. Tang, I. Babuschkin, S. Balaji, S. Jain, W. Saunders, C. Hesse, A. N. Carr, J. Leike, J. Achiam, V. Misra, E. Morikawa, A. Radford, M. Knight, M. Brundage, M. Murati, K. Mayer, P. Welinder, B. McGrew, D. Amodei, S. McCandlish, I. Sutskever, and W. Zaremba. Evaluating large language models trained on code. 2021.
- [4] K. Cobbe, V. Kosaraju, M. Bavarian, M. Chen, H. Jun, L. Kaiser, M. Plappert, J. Tworek, J. Hilton, R. Nakano, et al. Training verifiers to solve math word problems. *arXiv preprint arXiv:2110.14168*, 2021. doi: 10.48550/arXiv.2110.14168.
- [5] H. Duanmu, Z. Yuan, X. Li, J. Duan, X. ZHANG, and D. Lin. SKVQ: Sliding-window key and value cache quantization for large language models. In *First Conference on Language Modeling*, 2024. URL <https://openreview.net/forum?id=nI6JyFSnyV>.
- [6] L. Gao, J. Tow, B. Abbasi, S. Biderman, S. Black, A. DiPofi, C. Foster, L. Golding, J. Hsu, A. Le Noac’h, H. Li, K. McDonnell, N. Muennighoff, C. Ociepa, J. Phang, L. Reynolds, H. Schoelkopf, A. Skowron, L. Sutawika, E. Tang, A. Thite, B. Wang, K. Wang, and A. Zou. A framework for few-shot language model evaluation, 07 2024. URL <https://zenodo.org/records/12608602>.
- [7] A. Grattafiori, A. Dubey, A. Jauhri, A. Pandey, A. Kadian, A. Al-Dahle, A. Letman, A. Mathur, A. Schelten, A. Vaughan, A. Yang, A. Fan, A. Goyal, A. Hartshorn, A. Yang, A. Mitra, A. Srivankumar, A. Korenev, A. Hinsvark, A. Rao, A. Zhang, A. Rodriguez, A. Gregerson, A. Spataru, B. Roziere, B. Biron, B. Tang, B. Chern, C. Caucheteux, C. Nayak, C. Bi, C. Marra, C. McConnell, C. Keller, C. Touret, C. Wu, C. Wong, C. C. Ferrer, C. Nikolaidis, D. Allonsius, D. Song, D. Pintz, D. Livshits, D. Wyatt, D. Esiobu, D. Choudhary, D. Mahajan, D. Garcia-Olano, D. Perino, D. Hupkes, E. Lakomkin, E. AlBadawy, E. Lobanova, E. Dinan, E. M. Smith, F. Radenovic, F. Guzmán, F. Zhang, G. Synnaeve, G. Lee, G. L. Anderson, G. Thattai, G. Nail, G. Mialon, G. Pang, G. Cucurell, H. Nguyen, H. Korevaar, H. Xu, H. Touvron, I. Zarov, I. A. Ibarra, I. Kloumann, I. Misra, I. Evtimov, J. Zhang, J. Copet, J. Lee, J. Geffert, J. Vranes, J. Park, J. Mahadeokar, J. Shah, J. van der Linde, J. Billock, J. Hong, J. Lee, J. Fu, J. Chi, J. Huang, J. Liu, J. Wang, J. Yu, J. Bitton, J. Spisak, J. Park, J. Rocca, J. Johnstun, J. Saxe, J. Jia, K. V. Alwala, K. Prasad, K. Upasani, K. Plawiak, K. Li, K. Heafield, K. Stone, K. El-Arini, K. Iyer, K. Malik, K. Chiu, K. Bhalla, K. Lakhotia, L. Rantala-Yeary, L. van der Maaten, L. Chen, L. Tan, L. Jenkins, L. Martin, L. Madaan, L. Malo, L. Blecher, L. Landzaat, L. de Oliveira, M. Muzzi, M. Pasupuleti, M. Singh, M. Paluri, M. Kardas, M. Tsimpoukelli, M. Oldham, M. Rita, M. Pavlova, M. Kambadur, M. Lewis, M. Si, M. K. Singh, M. Hassan, N. Goyal, N. Torabi, N. Bashlykov, N. Bogoychev, N. Chatterji, N. Zhang, O. Duchenne, O. Çelebi, P. Alrassy, P. Zhang, P. Li, P. Vasic, P. Weng, P. Bhargava, P. Dubal, P. Krishnan, P. S. Koura, P. Xu, Q. He, Q. Dong, R. Srinivasan, R. Ganapathy, R. Calderer, R. S. Cabral, R. Stojnic, R. Raileanu, R. Maheswari, R. Girdhar, R. Patel, R. Sauvestre, R. Polidoro, R. Sumbaly, R. Taylor, R. Silva, R. Hou, R. Wang, S. Hosseini, S. Chennabasappa, S. Singh, S. Bell, S. S. Kim, S. Edunov, S. Nie, S. Narang, S. Rapparth, S. Shen, S. Wan, S. Bhosale, S. Zhang, S. Vandenhende, S. Batra, S. Whitman, S. Sootla, S. Collot, S. Gururangan, S. Borodinsky, T. Herman, T. Fowler, T. Sheasha, T. Georgiou, T. Scialom, T. Speckbacher, T. Mihaylov, T. Xiao, U. Karn, V. Goswami, V. Gupta, V. Ramanathan, V. Kerkez, V. Gonguet, V. Do, V. Vogeti, V. Albiero, V. Petrovic, W. Chu, W. Xiong, W. Fu, W. Meers, X. Martinet, X. Wang, X. Wang, X. E. Tan, X. Xia, X. Xie, X. Jia, X. Wang, Y. Goldschlag, Y. Gaur, Y. Babaei, Y. Wen, Y. Song, Y. Zhang, Y. Li, Y. Mao, Z. D. Coudert, Z. Yan, Z. Chen, Z. Papakipos, A. Singh, A. Srivastava, A. Jain, A. Kelsey, A. Shajnfeld, A. Gangidi, A. Victoria, A. Goldstand, A. Menon, A. Sharma, A. Boesenberg, A. Baeovski, A. Feinstein, A. Kallet, A. Sangani, A. Teo, A. Yunus, A. Lupu, A. Alvarado, A. Caples, A. Gu, A. Ho, A. Poulton, A. Ryan, A. Ramchandani, A. Dong, A. Franco, A. Goyal, A. Saraf, A. Chowdhury, A. Gabriel, A. Bharambe, A. Eisenman, A. Yazdan, B. James, B. Maurer, B. Leonhardi, B. Huang, B. Loyd, B. D. Paola, B. Paranjape, B. Liu, B. Wu, B. Ni, B. Hancock, B. Wasti, B. Spence, B. Stojkovic, B. Gamido, B. Montalvo, C. Parker, C. Burton, C. Mejia, C. Liu, C. Wang, C. Kim, C. Zhou, C. Hu, C.-H. Chu, C. Cai, C. Tindal, C. Feichtenhofer, C. Gao, D. Civin, D. Beaty, D. Kreymer, D. Li, D. Adkins, D. Xu, D. Testuggine, D. David, D. Parikh, D. Liskovich, D. Foss, D. Wang, D. Le, D. Holland, E. Dowling, E. Jamil, E. Montgomery, E. Presani, E. Hahn, E. Wood, E.-T. Le, E. Brinkman,

- E. Arcaute, E. Dunbar, E. Smothers, F. Sun, F. Kreuk, F. Tian, F. Kokkinos, F. Ozgenel, F. Caggioni, F. Kanayet, F. Seide, G. M. Florez, G. Schwarz, G. Badeer, G. Swee, G. Halpern, G. Herman, G. Sizov, Guangyi, Zhang, G. Lakshminarayanan, H. Inan, H. Shojanazeri, H. Zou, H. Wang, H. Zha, H. Habeeb, H. Rudolph, H. Suk, H. Aspegren, H. Goldman, H. Zhan, I. Damlaj, I. Molybog, I. Tufanov, I. Leontiadis, I.-E. Veliche, I. Gat, J. Weissman, J. Geboski, J. Kohli, J. Lam, J. Asher, J.-B. Gaya, J. Marcus, J. Tang, J. Chan, J. Zhen, J. Reizenstein, J. Teboul, J. Zhong, J. Jin, J. Yang, J. Cummings, J. Carvill, J. Shepard, J. McPhie, J. Torres, J. Ginsburg, J. Wang, K. Wu, K. H. U, K. Saxena, K. Khandelwal, K. Zand, K. Matosich, K. Veeraraghavan, K. Michelena, K. Li, K. Jagadeesh, K. Huang, K. Chawla, K. Huang, L. Chen, L. Garg, L. A. L. Silva, L. Bell, L. Zhang, L. Guo, L. Yu, L. Moshkovich, L. Wehrstedt, M. Khabsa, M. Avalani, M. Bhatt, M. Mankus, M. Hasson, M. Lennie, M. Reso, M. Groshev, M. Naumov, M. Lathi, M. Keneally, M. Liu, M. L. Seltzer, M. Valko, M. Restrepo, M. Patel, M. Vyatskov, M. Samvelyan, M. Clark, M. Macey, M. Wang, M. J. Hermoso, M. Metanat, M. Rastegari, M. Bansal, N. Santhanam, N. Parks, N. White, N. Bawa, N. Singhal, N. Egebo, N. Usunier, N. Mehta, N. P. Laptev, N. Dong, N. Cheng, O. Chernoguz, O. Hart, O. Salpekar, O. Kalinli, P. Kent, P. Parekh, P. Saab, P. Balaji, P. Rittner, P. Bontrager, P. Roux, P. Dollar, P. Zvyagina, P. Ratanchandani, P. Yuvraj, Q. Liang, R. Alao, R. Rodriguez, R. Ayub, R. Murthy, R. Nayani, R. Mitra, R. Parthasarathy, R. Li, R. Hogan, R. Battey, R. Wang, R. Howes, R. Rinott, S. Mehta, S. Siby, S. J. Bondu, S. Datta, S. Chugh, S. Hunt, S. Dhillon, S. Sidorov, S. Pan, S. Mahajan, S. Verma, S. Yamamoto, S. Ramaswamy, S. Lindsay, S. Lindsay, S. Feng, S. Lin, S. C. Zha, S. Patil, S. Shankar, S. Zhang, S. Zhang, S. Wang, S. Agarwal, S. Sajuyigbe, S. Chintala, S. Max, S. Chen, S. Kehoe, S. Satterfield, S. Govindaprasad, S. Gupta, S. Deng, S. Cho, S. Virk, S. Subramanian, S. Choudhury, S. Goldman, T. Remez, T. Glaser, T. Best, T. Koehler, T. Robinson, T. Li, T. Zhang, T. Matthews, T. Chou, T. Shaked, V. Vontimitta, V. Ajayi, V. Montanez, V. Mohan, V. S. Kumar, V. Mangla, V. Ionescu, V. Poenaru, V. T. Mihailescu, V. Ivanov, W. Li, W. Wang, W. Jiang, W. Bouaziz, W. Constable, X. Tang, X. Wu, X. Wang, X. Wu, X. Gao, Y. Kleinman, Y. Chen, Y. Hu, Y. Jia, Y. Qi, Y. Li, Y. Zhang, Y. Zhang, Y. Adi, Y. Nam, Yu, Wang, Y. Zhao, Y. Hao, Y. Qian, Y. Li, Y. He, Z. Rait, Z. DeVito, Z. Rosnbrick, Z. Wen, Z. Yang, Z. Zhao, and Z. Ma. The Llama 3 herd of models. *arXiv preprint arXiv:2407.21783*, 2024. doi: 10.48550/arXiv.2407.21783.
- [8] M. Hariri, A. Luo, W. Chen, S. Zhong, T. Zhang, Q. Wang, X. Hu, X. Han, and V. Chaudhary. Quantize what counts: More for keys, less for values. *arXiv preprint arXiv:2502.15075*, 2025. URL <https://arxiv.org/abs/2502.15075>.
- [9] C. Hooper, S. Kim, H. Mohammadzadeh, M. W. Mahoney, Y. S. Shao, K. Keutzer, and A. Gholami. KVQuant: Towards 10 million context length LLM inference with KV cache quantization. In A. Globerson, L. Mackey, D. Belgrave, A. Fan, U. Paquet, J. Tomczak, and C. Zhang, editors, *Advances in Neural Information Processing Systems*, volume 37, pages 1270–1303. Curran Associates, Inc., 2024. doi: 10.52202/079017-0040.
- [10] A. Q. Jiang, A. Sablayrolles, A. Mensch, C. Bamford, D. S. Chaplot, D. Casas, F. Bressand, G. Lengyel, G. Lample, L. Saulnier, et al. Mistral 7B. arxiv. *arXiv preprint arXiv:2310.06825*, 10:3, 2023. doi: 10.48550/arXiv.2310.06825.
- [11] H. Kang, Q. Zhang, S. Kundu, G. Jeong, Z. Liu, T. Krishna, and T. Zhao. GEAR: An efficient error reduction framework for KV cache compression in LLM inference. In M. Rezagholizadeh, P. Passban, S. Samiee, V. Partovi Nia, Y. Cheng, Y. Deng, Q. Liu, and B. Chen, editors, *Proceedings of The 4th NeurIPS Efficient Natural Language and Speech Processing Workshop*, volume 262 of *Proceedings of Machine Learning Research*, pages 305–321. PMLR, 14 Dec 2024. URL <https://proceedings.mlr.press/v262/kang24a.html>.
- [12] A. Lewkowycz, A. Andreassen, D. Dohan, E. Dyer, H. Michalewski, V. Ramasesh, A. Slone, C. Anil, I. Schlag, T. Gutman-Solo, Y. Wu, B. Neyshabur, G. Gur-Ari, and V. Misra. Solving quantitative reasoning problems with language models. In *Proceedings of the 36th International Conference on Neural Information Processing Systems*, NIPS ’22, Red Hook, NY, USA, 2022. Curran Associates Inc. ISBN 9781713871088. doi: 10.5555/3600270.3600548.
- [13] A. Liu, J. Liu, Z. Pan, Y. He, G. Haffari, and B. Zhuang. MiniCache: KV cache compression in depth dimension for large language models. In A. Globerson, L. Mackey, D. Belgrave,

- A. Fan, U. Paquet, J. Tomczak, and C. Zhang, editors, *Advances in Neural Information Processing Systems*, volume 37, pages 139997–140031. Curran Associates, Inc., 2024. doi: 10.52202/079017-4443. URL https://proceedings.neurips.cc/paper_files/paper/2024/file/fd0705710bf01b88a60a3d479ea341d9-Paper-Conference.pdf.
- [14] Z. Liu, J. Yuan, H. Jin, S. Zhong, Z. Xu, V. Braverman, B. Chen, and X. Hu. KIVI: A tuning-free asymmetric 2bit quantization for KV cache. *arXiv preprint arXiv:2402.02750*, 2024. doi: 10.48550/arXiv.2402.02750.
- [15] R. Pope, S. Douglas, A. Chowdhery, J. Devlin, J. Bradbury, J. Heek, K. Xiao, S. Agrawal, and J. Dean. Efficiently scaling transformer inference. In D. Song, M. Carbin, and T. Chen, editors, *Proceedings of Machine Learning and Systems*, volume 5, pages 606–624. Curran, 2023. URL https://proceedings.mlsys.org/paper_files/paper/2023/file/c4be71ab8d24cdfb45e3d06dbfca2780-Paper-mlsys2023.pdf.
- [16] R. Sanovar, S. Bharadwaj, R. S. Amant, V. Rühle, and S. Rajmohan. LeanAttention: Hardware-aware scalable attention mechanism for the decode-phase of transformers. In *Eighth Conference on Machine Learning and Systems*, 2025. URL <https://openreview.net/forum?id=KVZDNEoCOQ>.
- [17] Z. Su and K. Yuan. KVSink: Understanding and enhancing the preservation of attention sinks in KV cache quantization for LLMs. In *Second Conference on Language Modeling*, 2025. URL <https://openreview.net/forum?id=gIqb6zWZo0>.
- [18] S. Tehrani, W. Gao, and D. Sharma. Turboquant. <https://github.com/back2matching/turboquant>, 2026.
- [19] H. Touvron, L. Martin, K. Stone, P. Albert, A. Almahairi, Y. Babaei, N. Bashlykov, S. Batra, P. Bhargava, S. Bhosale, D. Bikel, L. Blecher, C. C. Ferrer, M. Chen, G. Cucurull, D. Esiobu, J. Fernandes, J. Fu, W. Fu, B. Fuller, C. Gao, V. Goswami, N. Goyal, A. Hartshorn, S. Hosseini, R. Hou, H. Inan, M. Kardas, V. Kerkez, M. Khabsa, I. Kloumann, A. Korenev, P. S. Koura, M.-A. Lachaux, T. Lavril, J. Lee, D. Liskovich, Y. Lu, Y. Mao, X. Martinet, T. Mihaylov, P. Mishra, I. Molybog, Y. Nie, A. Poulton, J. Reizenstein, R. Rungta, K. Saladi, A. Schelten, R. Silva, E. M. Smith, R. Subramanian, X. E. Tan, B. Tang, R. Taylor, A. Williams, J. X. Kuan, P. Xu, Z. Yan, I. Zarov, Y. Zhang, A. Fan, M. Kambadur, S. Narang, A. Rodriguez, R. Stojnic, S. Edunov, and T. Scialom. Llama 2: Open foundation and fine-tuned chat models. *arXiv preprint arXiv:2307.09288*, 2023. doi: 10.48550/arXiv.2307.09288.
- [20] H. Wang, L. Han, K. Xu, and A. Srivastava. Squat: Subspace-orthogonal KV cache quantization. *arXiv preprint arXiv:2503.24358*, 2025. doi: 10.48550/arXiv.2503.24358.
- [21] T. Wolf, L. Debut, V. Sanh, J. Chaumond, C. Delangue, A. Moi, P. Cistac, T. Rault, R. Louf, M. Funtowicz, J. Davison, S. Shleifer, P. von Platen, C. Ma, Y. Jernite, J. Plu, C. Xu, T. L. Scao, S. Gugger, M. Drame, Q. Lhoest, and A. M. Rush. Transformers: State-of-the-art natural language processing. In *Proceedings of the 2020 Conference on Empirical Methods in Natural Language Processing: System Demonstrations*, pages 38–45, Online, Oct. 2020. Association for Computational Linguistics. URL <https://www.aclweb.org/anthology/2020.emnlp-demos.6>.
- [22] G. Xiao, Y. Tian, B. Chen, S. Han, and M. Lewis. Efficient streaming language models with attention sinks. In *The Twelfth International Conference on Learning Representations*, 2024. URL <https://openreview.net/forum?id=NG7sS51zVF>.
- [23] A. Zandieh, M. Daliri, M. Hadian, and V. Mirrokni. Turboquant: Online vector quantization with near-optimal distortion rate. In *The Fourteenth International Conference on Learning Representations*, 2026. URL <https://openreview.net/forum?id=t03ASKZ1ok>.